Experiments on the Generation of Internal Waves in a Stratified Fluid

H. E. Gilreath* and A. Brandt†
Applied Physics Laboratory, Johns Hopkins University, Laurel, Maryland

This paper presents an overview of the results of an experimental study of internal gravity waves produced as a result of the motion of a self-propelled vehicle through a fluid in which the density varies with depth. Two ambient density profiles are considered: one for which the characteristic vertical length scale of the density change is large compared to the vehicle diameter, and a second in which this scale is smaller than the diameter. The most significant results show a strong coupling between wake turbulence and short, random internal waves. In the presence of sharp density gradients, the experiments reveal the onset of nonlinear influences on propagation, leading to the formation of solitary waves. Comparisons with theory are also presented.

Nomenclature

b = wake height
b_c = maximum wake height, at collapse point
C = wave speed
C_0 = limiting wave speed
D = reference length, vehicle diameter
F = Froude number
F_L = Froude number based on vehicle length
H = reference depth
k = horizontal or total wavenumber
L = vehicle length
N = Vaisala frequency
p = pressure
r,θ = radial and circumferential coordinates
t = time
u,v,w = local velocity components
U = reference velocity, vehicle velocity
V,W = initial values of transverse and vertical mean velocities
x,y,z = axial, transverse, and vertical coordinates
α = average density gradient in wake
β = ambient density gradient
δ = internal wave displacement
Δ = maximum wave amplitude
Δb = change in wake height
$\Delta\rho$ = density change across interface
θ_c = preferred direction of wave propagation in $y=0$ plane
Λ = interface thickness of sharp pycnocline
ν = source distribution
Ω = initial density perturbation
ρ = density
ρ_0 = reference density
$\bar{\rho}$ = average density
ω = frequency

Presented as Paper 83-1704 at the AIAA 16th Fluid and Plasma Dynamics Conference, Danvers, Mass., July 12-14, 1983; received Aug. 22, 1983; revision received Sept. 24, 1984.

*Chief Scientist, Submarine Technology Department.
†Hydrodynamics Group Scientist, Submarine Technology Department.

I. Introduction

IN this paper we present an overview of a set of experiments that deal with internal gravity waves produced as a result of the motion of a self-propelled vehicle through a stratified fluid—a fluid in which the density varies with depth. Because the propagation of waves of this kind is generally three-dimensional, anisotropic, and dispersive, the wave pattern can be very complicated even when the ambient density structure is relatively simple. Consequently, the usual first step in attempting to understand the motion is to divide the wavefield into source-associated components and consider each contribution independently. The two most familiar components are body-generated waves and wake-generated waves; the first being the result of the displacement of fluid by a solid object, and the second arising from the collapse of "mixed fluid" in its wake. Both of these sources have been studied extensively, e.g., Refs. 1-4.

To be more general, it should be pointed out that any localized disturbance to a stratified fluid will cause a transfer of energy into propagating modes to some degree, the relative amount depending upon the value of some representative internal Froude number, F. The Froude number, $F \equiv 2\pi U/ND$, can be thought of as the ratio of two time scales, one being the Vaisala period $(2\pi/N)$ and the other, the characteristic flow time, (D/U). In the preceding definition, N is the Vaisala frequency, $N \equiv [-(g/\rho)\ (d\rho/dz)]^{1/2}$, i.e., the intrinsic frequency of oscillation of a fluid element about its equilibrium position in a stratified medium; U is a reference velocity, and D a reference length. When an appropriately defined Froude number is of the order of unity, strong internal wave radiation is possible.

In the following sections, we will examine the total internal wavefield generated by a moving vehicle for two idealized cases—one for which the ambient density varies gradually (and the Vaisala frequency of the fluid is independent of depth), and the other for which the density change occurs suddenly across a thin interface. In the first of these cases, it will be necessary to account for the influence of swirl on the mean wavefield in addition to the body and wake sources noted earlier, since in these experiments the test vehicle is propeller driven. More important will be the consideration of a surprisingly large nondeterministic component of internal wave radiation associated with the quasiperiodic, large eddy structure of the turbulent wake, similar in some respects to the radiation of sound from high-speed turbulent flows.

These experiments are considerably distinct from previous studies of internal wave generation by turbulent flows, such as that of Townsend,[5] where a model of internal wave excitation by an atmospheric boundary layer is presented, and that of

Linden,[6] where mixed-layer deepening due to grid-induced turbulence is considered. Internal waves generated by a self-propelled body were briefly discussed in the study of the turbulent wake flow by Lin and Pao.[7]

In the second series of experiments, the results will show that the nature of internal wave propagation becomes increasingly pulse-like as the ambient density change becomes more abrupt, leading to the formation of "solitons," or particle-like waves. These solitary internal waves owe their existence to a balance between dispersive and nonlinear effects, dispersive effects tending to smooth an initial perturbation in opposition to the steepening tendency of nonlinear influences. Since the speed of propagation of an internal soliton is always greater than the maximum speed of an infinitesimal internal wave, a qualitative analogy can be drawn to a "shock wave."

The first results showing the propagation of solitary waves on a sharp density interface were reported by Davis and Acrivos,[8] using a pulse-type source. Further experiments in a stratified interface were performed by Hurdis and Pao[9] and Yates[10] and for an immiscible fluid interface by Koop and Butler.[11] The present experiments extend these results to the case of generation by a self-propelled body over a range of Froude numbers. Before discussing these results further, we will briefly describe the experimental methods and then introduce a few central theoretical concepts.

II. Experimental Methods

A. Towing Tank Facility

The experiments were conducted in the Applied Physics Laboratory (APL) Stratified Towing Tank Facility. The main tank is 30 ft long, 2 ft deep, and includes a 6-ft long by 6-ft wide test section at midtank length. The tank is filled by introducing a series of layers of saline solution through a slotted header which extends along the full length of the tank bottom. The ambient density profile in the tank is obtained by measuring the vertical variation of two state properties: specific conductance and temperature. These measurements are made by means of an automatic profiling apparatus, located just forward of the test section, that slowly (0.05 in./s) lowers a single-electrode conductivity probe and a small thermocouple through the fluid.

For the tests requiring the formation of a sharp density interface, a unique selective withdrawal system was developed which permitted the precise control of an otherwise rapidly changing ambient density profile.[12]

B. Self-Propelled Test Vehicle

The test vehicle is a 3-in.-diameter streamlined body with a length-to-diameter ratio of 12:1. The model is propelled by a 3-bladed, 1.5-in.-diam propeller which operates at 860 rpm when the model is self-propelled at 2 ft/s.

The complete model assembly is positively buoyant and is held at a selected depth in the fluid by a series of eight fine (0.004-in. diameter) stainless steel wires.

To minimize acceleration time, the model is towed at the speed it would eventually attain at the set propeller speed (the self-propelled point). This point is identified as the model speed for which there is no mean flow in the wake (zero net momentum), as discerned by shadowgraphic visualization methods.

C. Instrumentation and Measurement Techniques

Since the tank is stratified through the use of saline solutions of various concentrations, the specific conductance of the ambient fluid is a function of depth. This circumstance allows vertical displacement to be measured with a single-electrode conductivity probe, which in effect responds to conductance changes in the immediate vicinity of the small (0.001 in.) platinized electrode. In the present tests, probes of this type were mounted in various vertical and horizontal arrays between the model and the surface. The probes were calibrated in situ by raising and lowering the arrays through a series of selected displacements.

Single-electrode conductivity probes have very poor dynamic response characteristics unless provided with a mean flow.[13] The required motion is achieved by translating the carriage on which the instruments are mounted. Either of two schemes for moving the carriage is used depending upon whether the cross-track or down-track aspects of the wavefield are to be investigated. A high-speed, pneumatically driven carriage is used for cross-track measurements, a vertical array of probes being literally "fired" across the test section to obtain a snapshot of the wavefield at a selected distance aft of the vehicle. For downtrack measurements, the configuration of probes is slowly translated (0.5 in./s) along the axis of the tank. This low probe speed is still sufficient to overcome the response problem, and the need for troublesome and invariably inaccurate dynamic corrections is eliminated. The recorded data is latter referred to a body-fixed coordinate system. The second of the two methods was used for most of the experiments discussed in the present report.

The probe arrangement for the experiments in the sharply changing density field was substantially different from either of the preceding configurations. For these tests, the instrumentation consisted of two stationary, three-element vertical arrays of conductivity probes (centered on the midinterface depth), and a hot-film anemometer (located at the midinterface depth). The conductivity probe rakes were offset from the tank axis, and from each other, to provide timing indicators for determining the average wave speed. The relatively strong currents associated with nonlinear internal waves assure acceptable instrument response in a stationary configuration.

As it turns out, understanding internal wave radiation from a turbulent wake requires an examination of the motion of the interface between turbulent and nonturbulent fluid that defines the instantanous wake boundary. The development of the wake edge, in its vertical aspect, was recorded by shadowgraphic methods on motion picture film. The wake edge coordinates were digitized and later analyzed to obtain the wake height and its variance as functions of the distance behind the vehicle.

D. Experimental Approach and Testing Procedures

It was clear from the beginning of the experiments that the radiation of internal waves from a turbulent wake in a stratified medium is far more complicated than anyone had expected previously. Early tests disclosed an unmistakable degree of randomness in the wavefield, and further experimentation was shaped by the need for a statistical description of the results. In view of certain experimental limitations associated with stratified flow measurements, and given the inherent nonstationarity of the flowfield, we were led to adopt ensemble testing methods. These methods are based upon an examination of the variations in measurements over a large number of identical tests; an approach rarely used in fluid dynamical experiments due to the difficulties associated with repeating any experiment with adequate precision.

Applying ensemble methods in the present work made it necessary to control precisely the model motion, the ambient density profile, and the measurement system parameters. Procedures also needed to be developed to cancel the "noise" caused by natural background fluid motions. Furthermore, a considerable number of special tests were required to assess the influence of starting and stopping transients, the effects of disturbances from the submerged portion of the towing system, the sensitivity of results to small pitch and yaw angles and to slight departures from the self-propelled point, etc.

All factors considered, it was not possible to conduct more than about four tests per day and still achieve acceptable repeatability; and assembling a single ensemble required about

a month's time. Each set of data consisted of between 15 and 20 test records, carefully screened according to stringent measures of repeatability. As an illustration, the standard error, $\epsilon \equiv \sigma/n^{1/2}$ (calculated from the standard deviation σ and number of samples in the ensemble set), of approximately 2% of the peak potential flow displacement was achieved at $x/D = 20$, a region where a high degree of repeatability is expected. In terms of true displacement, this error corresponds to about 0.004 in.

Ensemble methods were not used in the experiments conducted in the step-like density field. Instead, the density structure was held fixed and a parametric series of tests was constructed by varying the vehicle speed.

III. Theoretical Considerations

A. Mean Wavefield

For the case in which the vehicle moves in a uniformly stratified medium (e.g., $N = \text{const}$) we assume that once generated the wavefield evolves in reasonable accordance with the linearized Navier-Stokes equations with the Boussinesq approximation.[14] We further invoke the slender body approximation, $(D/L)^2 \ll 1$, and assume that the Froude number F is very large, allowing $\partial u/\partial x$ to be neglected in the continuity equation. These linearized equations can be solved subject to initial conditions for u, v, w and ρ specified at $x = x_0$ and to the boundary conditions, $w = 0$ at $z = 0$, $-H$.

It remains to specify the source distribution and particular initial conditions. The large value of F allows us to approximate the body-generated disturbance by a source distribution corresponding to the potential flow around the vehicle in an unstratified medium. It is adequate to choose the distribution for a Rankine ovoid of source strength ν and slenderness ratio L/D, i.e.,

$$\nu(x,y,z) = \frac{\pi}{4} UD^2 \left[\delta\left(x + \frac{l}{2}, y, z+h\right) - \delta\left(x - \frac{l}{2}, y, z+h\right) \right] \tag{1}$$

where $l = L - D/2$ and the vehicle is located at a depth $z = -h$.

To examine the influence of wake collapse on the average wavefield, we assume that turbulent mixing produces a hydrostatic imbalance by lowering the average density gradient inside the wake with respect to the ambient. Hence, the general picture is one in which the wake at first grows radially—reaching a maximum height b_c at a distance x_c aft of the vehicle—and then collapses, decreasing in vertical extent and spreading rapidly in the horizontal as hydrostatic forces become predominant. The decrease in wake height ceases when the interior and exterior gradients are again equal.

The simplest model of this process represents the wake cross section at the point of maximum growth as a circle of radius b_c (Ref. 15). Within this circular region the fluid is assumed to be mixed to an extent described by the ratio α/β; where α is the mean density gradient inside the wake, and β is the ambient density gradient. Following Ref. 15, the term α/β can be estimated from a measurement of the amount of collapse:

$$1 - (\alpha/\beta) = \Delta b/b_c \tag{2}$$

where Δb is the difference between the wake heights at the beginning and end of collapse.

We expect a well-designed self-propelled vehicle to deposit little mean kinetic energy in its wake, and, therefore, to the simplest approximation, the initial conditions needed to compute wake-collapse generated waves are

$$V = W = 0 \tag{3}$$

$$\Omega = -\rho_0 \beta \left(1 - \frac{\alpha}{\beta}\right)(z+h); \quad r < b_c$$
$$= 0; \qquad r > b_c \tag{4}$$

where $r \equiv [y^2 + (z+h)^2]^{1/2}$. Both conditions are to be applied at $x = x_c$. Initialization for swirl effects is accomplished by specifying an initial angular velocity based on the known propeller performance conditions.

With these specifications, the linearized equations can be solved by standard integral transform methods.[4,14] The wavefield is thereby portrayed as a superposition of an infinite number of discrete vertical modes of oscillation—described by a family of eigenfunctions $\Phi_n(z)$—with the energy of each mode continuously distributed over the full spectrum of horizontal wavenumbers.

In obtaining numerical solutions, only the first forty modes were included over the horizontal wavenumber band, $0.0013 < kD \leq 33.5$. It was found that these choices allowed the important scales of motion to be resolved while discarding only a negligible amount of the total energy in the wavefield. Since the vehicle was operated at a depth equal to one half of the total fluid depth, only even modes contribute to the wavefield.

B. Random Wavefield

Since we will later argue that the pronounced degree of randomness in the wave displacement data implies that the wavefield is highly unsteady, it is useful to consider briefly several theoretical aspects of time-dependent stratified flows. This subject has received considerable attention in the literature, but for present purposes we will refer only to the general linear theory of anisotropic wave motion present by Lighthill in Ref. 16.

Lighthill has given a general recipe for computing the kinematic pattern of the waves at large distances from the source. Omitting the details, the points of constant phase are found from

$$r = \phi(\nabla G/k \cdot \nabla G) \tag{5}$$

where ϕ is a constant identifying the phase ($\phi = 2\pi$, 4π, etc.), ∇ the gradient operator in wavenumber space, and G the dispersion relation. Lighthill further requires that the radiation condition be satisfied

$$\frac{r \cdot \nabla G}{\partial G/\partial \omega} > 0 \tag{6}$$

assuring that the waves have an outward velocity of energy propagation along a radius vector from the source.

The coordinates of lines of constant phase that define the wavefield are obtained from Eqs. (5) and (6). In general, these phase lines exhibit both divergent and transverse components that merge to form cusps. The wave amplitudes are highest in the vicinity of these cusps, and the rate of decay is lowest along the directions defined by their loci, and in this sense, the loci of cusps can be associated with preferred directions of propagation. When $\omega_0/N \gg 1$, the line of preferred direction in the plane of $y = 0$ has the slope

$$\Theta_c = \tan^{-1}[0.4(\omega_0/N)^{-1}] \tag{7}$$

This result will prove useful later in interpreting the geometry of the random wavefield.

C. Nonlinear Waves

We now turn our attention to several theoretical aspects of the experiments involving motion along a sharp density interface. If the scale of the vehicle-induced perturbations is large compared to the interfacial thickness, the resulting waves are "long" and, therefore, only weakly dispersive. If, at the same time, the waves are sufficiently steep, nonlinear effects can accumulate, tending to offset the weak dispersive tendencies. When an exact balance between dispersion and nonlinearity is achieved, the wave propagates with permanent form, i.e., becomes a solitary wave.

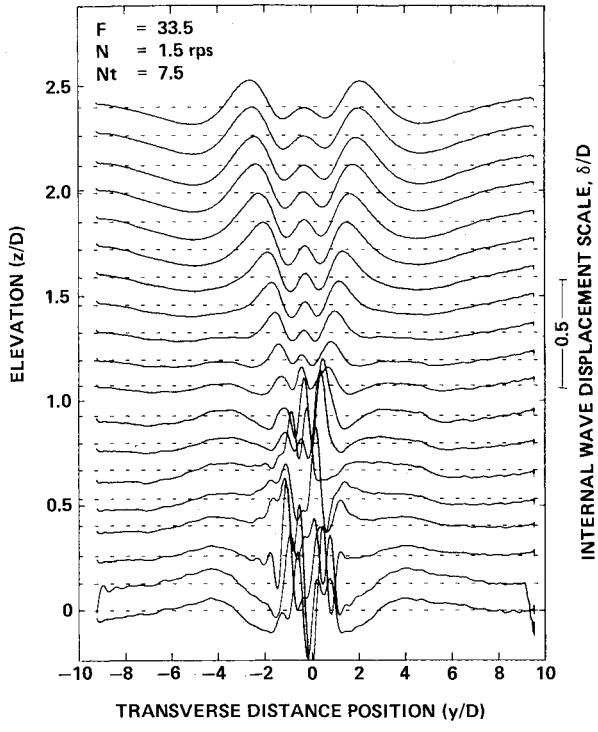

Fig. 1 Transverse wave pattern.

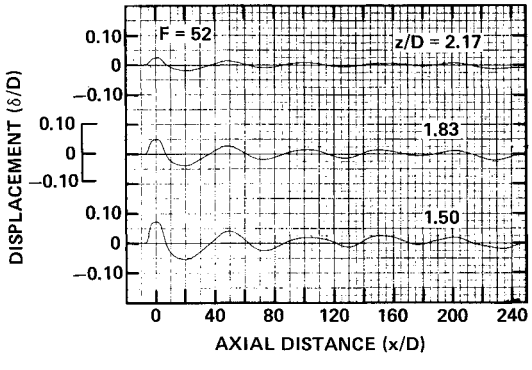

Fig. 2 Ensemble-average vertical displacements, $y/D=0$.

References 17 and 18 consider small amplitude solitary waves in stratified fluids for which the interfacial thickness is very small compared to the total depth, the situation of interest herein. Explicit results are given in the case of a hyperbolic tangent ambient density profile. The waveform of a second mode wave resembles a "bulge," of amplitude Δ, traveling along the interface and is described by

$$\frac{\delta}{\Lambda}=\tanh\left(\frac{z}{\Lambda}\right)\left[\frac{\lambda^2}{y^2+\lambda^2}\right]\frac{\Delta}{\Lambda} \tag{8}$$

where $\lambda=2.5\ \Lambda/(\Delta/\Lambda)$, Λ is a characteristic length scale, and y is measured in a wave-fixed coordinate system. The steady-state speed of propagation C can be shown to be

$$(C/C_0)^2=1+0.6(\Delta/\Lambda) \tag{9}$$

where $C_0^2=\delta\Delta\rho\Lambda/4\bar{\rho}$ is the limiting speed of a linear second-mode internal wave in the given density field. It is observed that the speed of propagation of a solitary wave depends upon its amplitude and always exceeds the linear limit.

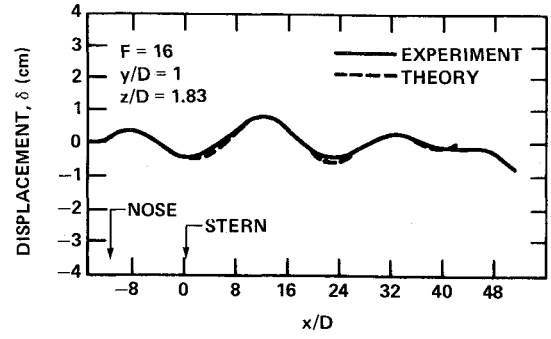

Fig. 3 The body generated component.

IV. Discussion of Results

A. Ensemble-Averaged Wavefield

Before we discuss specific results, it may be worthwhile for the reader to form a conceptual picture of the wavefield by examining Figs. 1 and 2. The first figure shows the crosstrack wave pattern measured using the high-speed instrument carriage. For this particular test, the model was towed without propulsion, and the relatively low value of F tended to suppress the wake-generated wave component considerably. These conditions act to simplify the picture, but the fan-like appearance of the internal wave-displacement pattern is nonetheless typical of radiation patterns behind vehicles moving in uniformly stratified fluids. As time progresses, more crests and troughs develop in the pattern, so that the fan appears to open as waves propagate away from the axis. As a consequence, the pattern in a horizontal plane is also "vee-shaped," albeit somewhat complex due to the multiplicity of modes and wavelengths. Waves of higher mode number and shorter wavelength travel more slowly and reside in a narrow wedge behind the vehicle. The entire wavefield is confined to a horizontal sector having a half-angle equal to $\Theta_0=\sin^{-1}(C_0/U)$.

The downstream evolution of the vertical displacements measured directly above the axis is shown in Fig. 2. These results represent an average over an 18-member ensemble, measured with the low-speed instrument carriage. The sharp elevation centered at $x/D=0$ is due to the "potential flow" around the vehicle. Thereafter, the wave-amplitude envelope falls off according to a $-\frac{1}{2}$ power law, in agreement with linear theory.

To analyze the wavefield in more detail, we need to isolate from each other the components generated by the body, wake collapse, and propeller swirl. We begin by noting that the theoretical specification of the disturbance due to the body alone does not suffer nearly the same degree of uncertainty as the other two. Figure 3 shows the result of a comparison of experiment and theory (cf., Sec. III) for a towed body operating at a low Froude number. The experimental arrangement was again chosen so that propeller effects were nonexistent and wake growth and collapse were greatly inhibited. Despite the fact that the body shape was approximated as a Rankine ovoid, and the displacement effects of the boundary layer and wake were ignored, the close correspondence makes it reasonable to consider separating the body and wake internal wavefields simply by subtracting the predictions of the theory for body waves from the average experimental waveforms. This procedure has proven to be useful and has been applied at higher values of F where wake effects cannot be ignored.

Once this step is taken, however, the problem remains of separating collapse-generated waves from those produced by propeller swirl. Here we can take advantage of the fact that, according to theory, the former component is symmetric with respect to the y axis, while the latter is antisymmetric. The asymmetry results from the sense of rotation of the single propeller. By locating probes at identical locations on either side of the vehicle track, we can reduce the wave records into even

and odd parts

$$\delta_{odd} = \tfrac{1}{2}[\delta(y) - \delta(-y)]$$

$$\delta_{even} = \tfrac{1}{2}[\delta(y) + \delta(-y)]$$

and thereby arrive at experimental estimates of each of the two wake components.

Initializing the theory for the collapse-generated waves requires information about the mean wake radius and the extent of collapse, as we noted in the preceding section. Figure 4 shows an example of the ensemble-averaged results obtained from wake shadowgraph data that was used to supply this information. The small amount of collapse implies that the fluid in the wake is far from completely mixed.

Examples of the overall results of these analysis procedures are given in Fig. 5. We can see that the experimental estimate of the collapse-generated wavefield (Fig. 5a) is in striking agreement with the theoretical waveform; but, amplitudes differ by more than a factor of two. Recalling the model described in Sec. III, the excess potential energy per unit length of wake at the point of collapse is given by

$$PE = \frac{\pi}{8}\rho_0 N^2 b_c^4 \left(1 - \frac{\alpha}{\beta}\right)^2$$

This relation indicates that the wave energy (and, hence, the square of the wave amplitude) is very sensitive to the model parameters (b_c, $\Delta b/b_c$) used to initialize the calculations.

The comparison between theory and experiment for the swirl-induced component (Fig. 5b) is rather poor. The results seem to suggest that coherent swirl energy in the wake is relatively short lived, leading to only a short pulse of internal waves before succumbing to turbulent dissipation. Linear theory, of course, incorporates no such complexity.

B. Nondeterministic Component

The presentation in Fig. 6 is a superposition of 18 identical runs recorded from one of the probes in an array directly above the vehicle track. The ensemble-average of these runs was shown earlier in Fig. 2. The reader will note that, with a few exceptions, the waveforms are essentially coincident up to $x/D = 50$, but thereafter the superimposed records become increasingly disorganized. In no sense can the results be said to be repeatable.

We can gain a better appreciation for the nature of the random variations by subtracting the average waveform from each of the records in Fig. 6 and replotting the results in superimposed form. This replotting has been done in Fig. 7 for data from the three probes in the vertical array.

The important feature to note is the spatial order that emerges when the three sets of random components are viewed side by side. As one follows the records along the x axis, there appears to be a fairly abrupt transition from reasonable steady (repeatable) flow to highly unsteady (nonrepeatable) flow. This transition point occurs progressively further downstream as the vertical distance from the track of the vehicle increases. For descriptive purposes, we refer to the surface formed by the transition points as the "transition front." Ahead of this imaginary surface, the flow is nearly steady, while behind it the flow is unsteady to a substantial degree. The slope of a line of preferred direction of propagation, discussed in Sec. III, is shown superimposed upon the random wave records, where $\omega_0/N = 50$ has been chosen to characterize the principal frequency of a presumed unsteady source. This slope can be seen to align reasonably well with the transition front.

The choice of $\omega_0/N = 50$ in comparing the theoretical envelope of an unsteady wavefield to the observed transition front is based upon the hypothesis that the random waves result from motions induced by large, quasiperiodic eddies in the turbulent wake. In simple terms, the argument is as follows. Free turbulent flows have highly convoluted bound-

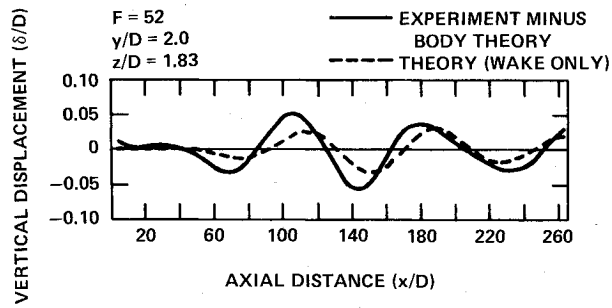

Fig. 5a The wake-collapse generated component.

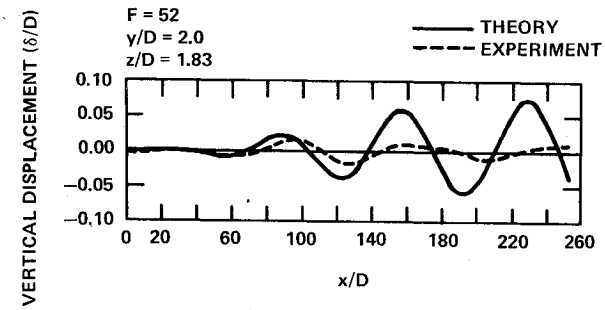

Fig. 5b The propeller swirl generated component.

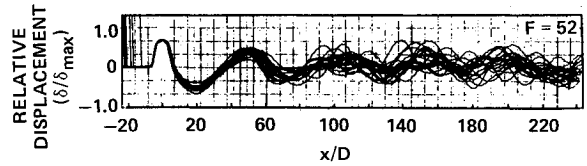

Fig. 6 Superposition of all test results, $y/D = 0$, $z/D = 1.5$.

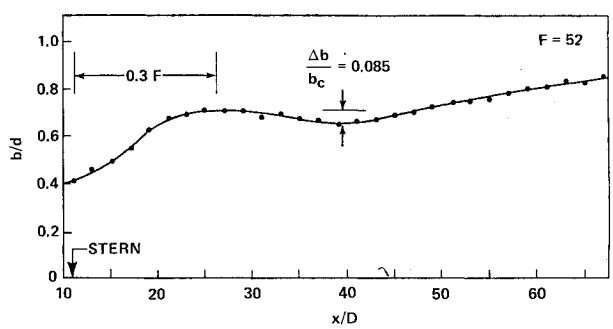

Fig. 4 Ensemble-averaged wake height.

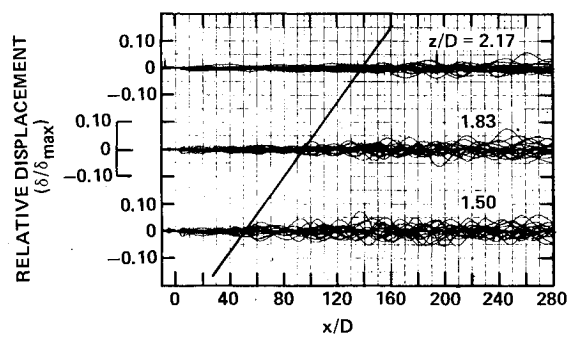

Fig. 7 Superimposed random displacement components, $y/D = 0$.

aries as a consequence of an intermittent structure best described as regular series of turbulent "bursts." The series of shadowgraphs shown in Fig. 8 illustrates the development of these bursts of turbulence as observed in the present experiments. The vertical lines in the photographs are spaced at $0.5D$ intervals, and it can be seen that "puffs" occur roughly one diameter apart. The burst frequency that would produce a separation of one diameter is U/D, from which we infer a predominant frequency of large eddy formation of $\omega_0/N = 50$ for the particular experiments at issue.

Following their violent rise in the near field, the turbulent puffs collapse under the influence of buoyancy forces, as shown in the lower photographs of Fig. 8. The standard deviation of the wake boundary is a measure of the average amplitude of the puffs, and the variation of this quantity with downstream distance is shown in Fig. 9. For the conditions of this particular experiment, an average puff grows to about 20% of the maximum wake radius before collapsing.

One presumes the wholesale conversion of turbulent kinetic energy to turbulent potential energy, and thence to random internal waves, occurs when an appropriate turbulence Froude number $u'/N\lambda_t$ (based on the rms turbulent velocity u' and the turbulent integral scale λ_t) approaches unity. From another aspect, one might expect this transfer to be maximally effective when the predominant frequency of the turbulence matches the intrinsic frequency of the medium N, in some sense. A limited series of experiments in which the Froude number was varied parametrically seems to reveal the possibility of such a resonance phenomenon, as evidenced by the variation of energy density of the random waves shown in Fig. 10. Since a least squares fit to the data suggests that the variance σ^2 increases logarithmically with F, the indicated functional form for energy density $(\ell n\, F)/F^2$, follows. In view of the small amount of data available, however, the reader should regard these latter results as preliminary.

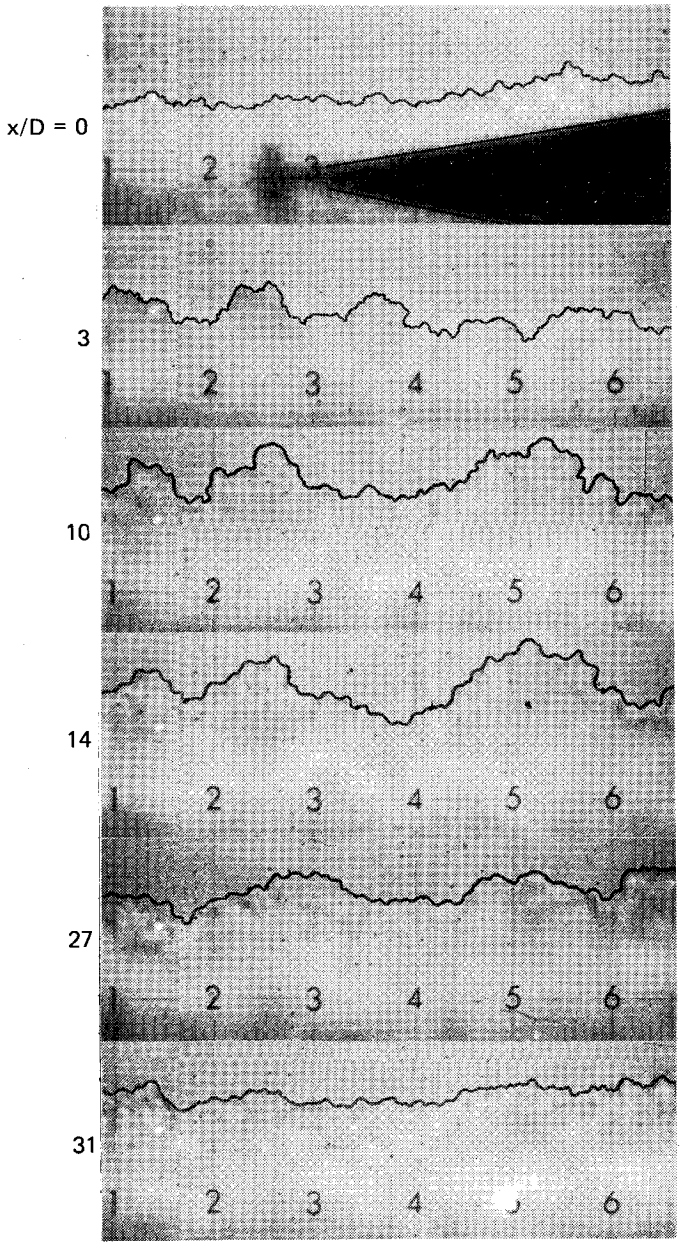

Fig. 8 Sequence of shadowgraphs of the wake.

C. Formation of Solitary Waves

In this last section we consider the results of the experiments conducted in a sharply changing density field. In these tests, the vehicle was towed (without propulsion) at a depth that coincided with the mean interface depth. The hyperbolic tangent profile described in Sec. III was found to provide an excellent representation of the experimental density profile when the length scale Λ was taken to be equal to $(g/2)\,(\Delta\rho/\bar{\rho})N^2_{\max}$, $N_{\max}$ being the maximum value of N. The internal Froude number, $F_L = 2\pi U/LN_{\max}$, was the major parameter varied during the tests.

When the interfacial thickness was sufficiently small compared to the model diameter ($\Lambda/D \leq 0.2$), solitary waves were clearly observed over the full range of Froude numbers covered by the tests ($0.7 < F_L < 2.5$). For all tests, only a single, second-mode (i.e., symmetric displacement about interfacial region) solitary wave was obvious in the data. Figure 11 shows the pulse-like signal recorded by a hot-film anemometer fixed at the midinterface depth and located $4.7D$ off the axis of travel. That the pulse shape does not change appreciably during propagation can be judged by noting the compact form of the wall-reflected signal. The wavefield was found to be extremely complex, and the identification of solitary waves less certain, when Λ/D exceeded a value of about 0.3.

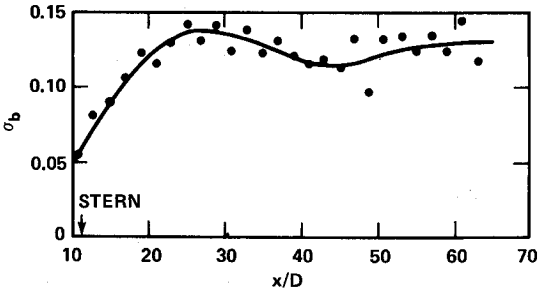

Fig. 9 Standard deviation of wake boundary.

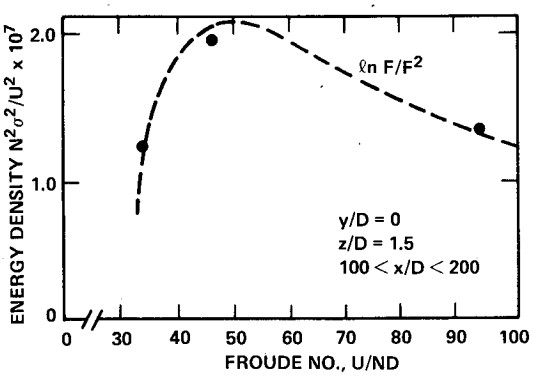

Fig. 10 Energy density of the random internal wave component.

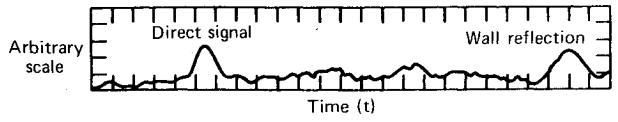

Fig. 11 Hot-film anemometer record of an internal soliton $F_L = 0.72$; $\Lambda/D = 0.14$.

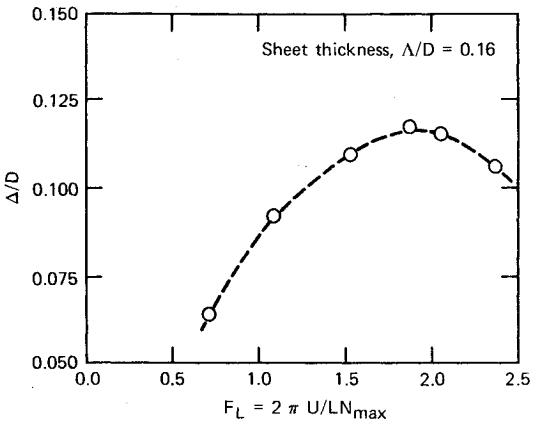

Fig. 12a Soliton amplitude as a function of Froude number.

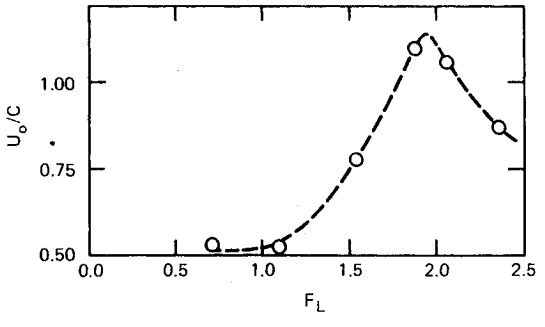

Fig. 12b Ratio of current to speed of propagation as a function of Froude number.

The results suggest several significant influences of Froude number. The peak wave displacement Δ appears to reach a maximum at a Froude number of about two, as illustrated in Fig. 12a. Expressed as a fraction of the interface thickness, the largest amplitudes are first order quantities, falling well outside the expected domain of the weakly nonlinear theory discussed in Sec. III.

The maximum current u_0 measured at the midinterface location also appears to peak around $F_L = 2$ (Fig. 12b). By using the average speed of propagation as the nondimensionalization factor (measured by timing the pulse between two probe arrays), we note that u_0/C at times exceeds unity, attesting to the occurrence of stagnation points and recirculation in a wave-fixed reference frame. This result was later confirmed by dye visualization experiments, which clearly showed the entrainment and transport of dyed wake fluid within the recirculation cells of the waves. The measurements of the speed of propagation demonstrated that the waves are supercritical ($C/C_0 > 1$) as they must be to qualify as solitary waves. The wave speed, however, was not well predicted by Eq. (9) when Δ/Λ was greater than about 0.3, the measured values being considerably higher. The wave shape also tended to be substantially more compact than described by Eq. (8). Both results speak to a high degree of nonlinearity in the observed waves.

Finally, we should point out that these waves were found to be persistent and nearly impervious to collisions with tank walls or with themselves. In this respect they merit being called, "solitons."

V. Conclusions

The present experiments have produced a set of ensemble-averaged data that can provide an accurate benchmark for testing the available theory for vehicle-induced internal wavefields. Unfortunately, the simplest framework, linear theory, has been found to suffer considerable shortcomings, the major exception being the excellent agreement found for the body-generated component.

Since the mean density and velocity fields downstream of the vehicle develop under the action of intense turbulent processes, the generation of internal waves by the wake is an inherently nonlinear phenomenon, even though the propagation of the waves may well be adequately represented by linear theory. The attempt to circumvent the nonlinear aspects of the flow by postulating simple source models has been seen to be only marginally successful; the outcome is better for the collapse mechanism than for the swirl mechanism. Although model "tuning" is always possible, a full nonlinear numerical treatment is probably needed to achieve substantial improvements in the prediction of general flows of this type.

Perhaps the most significant result of the ensemble experiments was the discovery of large variations in the wave structure from one test to the next, even though the test conditions were very nearly identical. The data, together with considerations of unsteady theory, can be used to build a fairly strong case of circumstantial evidence tying the random component of the wavefield to a quasiperiodicity in the structure of the turbulent wake. We have inferred from these results that, under certain circumstances, wake turbulence couples strongly into random internal waves, and that these waves exhibit preferred directions of propagation associated with the frequency composition of the turbulence.

No adequate methods exist for predicting turbulence-generated internal waves, but in a similar context, Lighthill[19] has considered the radiation of sound waves from compressible turbulent flows. The basic approach is to regard the nonlinear terms that describe the turbulence as forcing functions for the linear wavefield, assuming that the radiated energy is small compared to the energy content of the source region. However, as we have seen, this last assumption is unlikely to be valid in the case of internal wave radiation. Because the radiation results in a drastic change in the turbulence structure, direct computer simulations of the full, time-dependent, Navier-Stokes equations may be required to handle these flows.[20]

The experimental observation of solitary waves demonstrates that the influences of nonlinearity on the propagation of internal waves can produce major, even qualitative, changes in the wavefield when the characteristic scale of the ambient density field is smaller than the dimensions of the vehicle. Over much of the parametric range covered by the tests the amplitudes of the waves were clearly outside the regime of applicability of weakly nonlinear theory, and considerable mass transport and recirculation were found to occur at the highest amplitudes. Again, an adequate theoretical treatment demands the use of fully nonlinear numerical methods, but in view of the need to maintain a delicate balance between dispersion and nonlinearity, these methods must have exceedingly high fidelity.

Acknowledgments

The authors greatly appreciate the assistance of Dr. C. L. Yates and C. R. Walton in the development and conduct of these experiments. Much of the experimental methodology was developed in parallel with efforts at Flow Research, Inc. by Drs. Y-H Pao and J-T Lin; the authors are appreciative of their contributions. The analytical background and computer program for solution of the linearized equations was originally developed by Dr. M. Milder (unpublished) and further extend-

ed by Drs. D.R.S. Ko, J. J. Riley, M. C. Smithmeyer, and R. E. Robins at Flow Research, Inc. and, subsequently, by Dr. G. Dailey at JHU/APL. These efforts are also much appreciated.

References

[1]Hudimac, A. A., "Ship Waves in a Stratified Ocean," *Journal of Fluid Mechanics*, Vol. 11, 1961, pp. 229-243.

[2]Keller, J. B. and Munk, W. H., "Internal Wave Wakes of a Body Moving in a Stratified Fluid," *Physics of Fluids*, Vol. 13, 1970, pp. 1425-1431.

[3]Schooley, A. and Stewart, R., "Experiments with a Self-Propelled Body Submerged in a Fluid with a Vertical Density Gradient," *Journal of Fluid Mechanics*, Vol. 15, 1963, pp. 83-96.

[4]Miles J. W., "Internal Waves Generated by a Horizontally Moving Source," *Journal of Geophysics Fluid Mechanics*, Vol. 2, 1971, pp. 63-87.

[5]Townsend, A. A., "Excitation of Internal Waves by a Turbulent Boundary Layer," *Journal of Fluid Mechanics*, Vol. 22, 1965, pp. 241-252.

[6]Linden, P. F., "The Deepening of a Mixed Layer in Stratified Fluid," *Journal of Fluid Mechanics*, Vol. 71, 1975, pp. 385-405.

[7]Lin, J-T and Pao, Y-H, "Wakes in Stratified Fluids," *Annual Review of Fluid Mechanics*, Vol. 11, 1979, pp. 317-338.

[8]Davis, R. E. and Acrivos, A., "Solitary Internal Waves in Deep Water," *Journal of Fluid Mechanics*, Vol. 29, 1967, pp. 593-607.

[9]Hurdis, D. A. and Pao, H-P, "Experimental Observation of Internal Solitary Waves in a Stratified Fluid," *Physics of Fluids*, Vol. 18, 1975, pp. 385-386.

[10]Yates, C. L., "An Experimental Study of Internal Solitary Waves," AIAA Paper, Huntsville, Ala., Jan. 1978.

[11]Koop, C. G. and Butler, G., "An Investigation of Internal Solitary Waves in a Two-Fluid System," *Journal of Fluid Mechanics*, Vol. 112, 1981, pp. 225-251.

[12]Gilreath, H. E., "The Establishment and Control of Density Microstructure in Stratified Flow Experiments," *Experiments in Fluids*, Vol. 1, 1983, pp. 210-212.

[13]Gilreath, H. E. and Walton, C. R., "Frequency Response of Stationary Internal Wave Probes," *Journal of Hydronautics*, Vol. 7, 1973, pp. 170-172.

[14]Yih, C.-S., "Stratified Flows," *Annual Reviews of Fluid Mechanics*, Vol. 1, 1969, pp. 73-110.

[15]Hartman, R. J. and Lewis, H. W., "Wake Collapse in a Stratified Fluid: Linear Treatment," *Journal of Fluid Mechanics*, Vol. 51, 1972, pp. 613-618.

[16]Lighthill, M. J., "Studies on Magneto-Hydrodynamic Waves and Other Anisotropic Wave Motions," *Philosophical Transactions of the Royal Society of London*, No. A252, 1960, pp. 397-430.

[17]Benjamin, T. B., "Internal Waves of Finite Amplitude and Permanent Form," *Journal of Fluid Mechanics*, Vol. 25, 1966, pp. 241-270.

[18]Ono, H., "Algebraic Solitary Waves in Stratified Fluids," *Journal of the Physics Society of Japan*, Vol. 39, 1975, p. 1082.

[19]Lighthill, M. J., "On Sound Generated Aerodynamically: General Theory," *Proceedings of the Royal Society of London*, Vol. A211, 1952, p. 564.

[20]Riley, J. J. and Metcalfe, R. W., "Direct Numerical Simulations of the Turbulent Wake of an Axisymmetric Body," *Turbulent Shear Flows 2*, edited by L.J.S. Bradbury, et al., Springer-Verlag, New York, 1980, p. 78.